

Accepted Manuscript

Synthesis, crystal structure and DNA/protein binding of tetranuclear Cu(II) complexes with a double-open-cubane like core framework

Aparup Paul, Horst Puschmann, Subal Chandra Manna

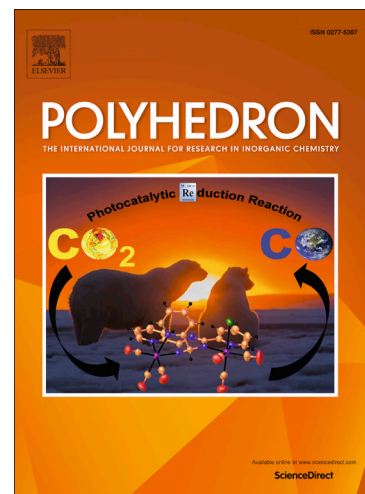
PII: S0277-5387(18)30485-6
DOI: <https://doi.org/10.1016/j.poly.2018.08.020>
Reference: POLY 13343

To appear in: *Polyhedron*

Received Date: 3 April 2018
Accepted Date: 2 August 2018

Please cite this article as: A. Paul, H. Puschmann, S. Chandra Manna, Synthesis, crystal structure and DNA/protein binding of tetranuclear Cu(II) complexes with a double-open-cubane like core framework, *Polyhedron* (2018), doi: <https://doi.org/10.1016/j.poly.2018.08.020>

This is a PDF file of an unedited manuscript that has been accepted for publication. As a service to our customers we are providing this early version of the manuscript. The manuscript will undergo copyediting, typesetting, and review of the resulting proof before it is published in its final form. Please note that during the production process errors may be discovered which could affect the content, and all legal disclaimers that apply to the journal pertain.



Synthesis, crystal structure and DNA/protein binding of tetranuclear Cu(II) complexes with a double-open-cubane like core framework

Aparup Paul,^a Horst Puschmann,^b and Subal Chandra Manna*^a

^a*Department of Chemistry and Chemical Technology, Vidyasagar University, Midnapore 721102, West Bengal, India, E-mail: scmanna@mail.vidyasagar.ac.in, Fax: (91) (03222) 275329.*

^b*Department of Chemistry, University of Durham, South Road, Durham DH1 3LE, U.K.*

Abstract

The copper(II) complexes $[\text{Cu}_4(\text{L})_2(\text{HL})_2(\text{H}_2\text{O})_2] \cdot 2(\text{ClO}_4) \cdot 2(\text{H}_2\text{O}) \cdot \text{DMF}$ (**1**) and $[\text{Cu}_4(\text{L})_2(\text{HL})_2(\text{H}_2\text{O})_2] \cdot (\text{tp})$ (**2**) [H_2L = 2-ethoxy-6-[(1-hydroxymethyl-propylimino)-methyl]-phenol; tp = terephthalate] have been synthesized and characterized by single crystal X-ray diffraction and spectroscopic studies. The structural determination reveals that both the complexes are tetranuclear with a double-open-cubane like core framework. The 2D supramolecular structure of **1** and 3D supramolecular structure of **2** are formed through C-H... π and hydrogen bonding interactions, respectively. At room temperature both the complexes exhibit fluorescence with quantum yields of 0.41 and 0.40. The interactions of the complexes with calf thymus DNA (CT-DNA) and serum albumins were investigated using electronic absorption and fluorescence spectroscopic techniques. The studies reveals that the binding affinities of **1** and **2** with CT-DNA are of the order $8.86 \times 10^5 \text{ M}^{-1}$ and $7.14 \times 10^5 \text{ M}^{-1}$, respectively. Additionally, the interaction of the complexes with bovine serum albumin and human serum albumin were studied and the number of binding sites and binding constants were calculated using a double logarithm regression equation. The redox activities of the complexes were investigated in methanol solution by cyclic voltammetry.

Keywords: Tetranuclear copper(II); Double-open-cubane; Crystal structure; CT-DNA binding; Serum albumin binding

1. Introduction

Transition metal clusters containing paramagnetic metal ions represent an important class of compounds for their potential application in the area of molecular magnetism [1] and their importance in the field of bioinorganic chemistry, as mimics for multi-metal active sites of metalloproteins [2]. Polynuclear copper complexes of various structures, e.g. dimeric [3a], square planar [3b], cyclic [3c], pin-wheel [3d], roof-shaped [3e] and cubane types [3f-3j], are reported in the literature due to their potential application in the area of magnetism [4], catalysis [5] and bioinorganic modelling [6]. Depending on the arrangement of the copper and oxygen atoms in the Cu_4O_4 unit various cubane geometries, such as regular cubane [7], single-open cubane [8], double open cubane [9] and face-sharing dicubane, have been reported [9b,10] in the literature. A literature survey reveals that many copper(II) based coordination compounds are used as metallo-pharmaceuticals [11] and these compounds play an important role in biology due to their antimicrobial [12], antifungal [13], antibacterial [14], antitumoral [15], antiviral [16], antipyretic [13a] and antidiabetic activities [17]. DNA is the primary intracellular target of antitumor drugs, since the interaction between small molecules with DNA can cause DNA damage and block DNA synthesis in cancer cells [18]. Therefore, under physiological conditions, metal complexes which are capable of binding and cleaving DNA are considered as potential candidates for use as therapeutic agents in medicinal applications [19]. On the other hand, studies of the binding of metal complexes with serum albumins is important to understand the potential of these compounds as drugs, as the nature and magnitude of the binding has a direct relation on drug delivery, drug absorption and the therapeutic efficiency [20]. Therefore, understanding and characterizing the interaction of drugs with DNA and serum albumin (HSA/BSA) are important for the development of new

drugs. It is to note that the reported tetranuclear Cu(II)-cubane complexes mainly focused on the synthesis and magneto-structure correlation [4], whilst studies of the DNA/protein binding of tetranuclear Cu(II)-cubane complexes are rare in the literature [3g,3h].

As a part of our continuing work on Cu(II) complexes with Schiff base ligands, in the present contribution we have used a polydentate ligand (H_2L), which functions as a chelating ligand with its versatile coordination modes (Scheme 1), and using H_2L we synthesized two tetranuclear copper(II) complexes, $[Cu_4(L)_2(HL)_2(H_2O)_2] \cdot 2(ClO_4) \cdot 2(H_2O) \cdot DMF$ (**1**) and $[Cu_4(L)_2(HL)_2(H_2O)_2] \cdot (tp)$ (**2**) with a double open cubane structure. Interactions of the complexes with calf thymus DNA (CT-DNA) and serum albumins (BSA/HSA) have been studied with UV-vis and fluorescence spectroscopic techniques.

2. Experimental

2.1. Materials and physical measurements

High purity 2-amino-1-butanol, 2-hydroxy-3-ethoxybenzaldehyde, calf thymus DNA, bovine serum albumin and human serum albumin were purchased from Aldrich Chemical Co. Inc. and used as received. All other chemicals used were analytical grade. Solvents used for the spectroscopic studies were purified and dried by standard procedures before use [21].

Elemental analyses (carbon, hydrogen and nitrogen) were performed using a Perkin-Elmer 240C elemental analyzer. IR spectra were recorded as KBr pellets on a Bruker Vector 22FT IR spectrophotometer operating from 400 to 4000 cm^{-1} . The NMR spectra of the ligand were recorded on A Bruker 400 MHz instrument. ESI-MS spectra of the compounds and HL in methanol were recorded on an Agilent Q-TOF 6500 mass spectrometer and the software used for mass analysis was Mass hunter. Electronic absorption spectra were obtained with a Shimadzu UV-1601 UV-vis spectrophotometer at room temperature. Quartz cuvettes with a 1

cm path length and a 3 cm³ volume were used for all measurements. Emission spectra were recorded on a Hitachi F-7000 spectrofluorimeter. Room temperature (300 K) spectra were obtained in a methanolic solution using a quartz cell of 1 cm path length. The slit width was 5 nm for both excitation and emission.

The fluorescence quantum yield was determined using phenol as a reference and methanol medium for both the complexes and the reference. Emission spectra were recorded by exciting the complex and the reference phenol at the same wavelength, maintaining nearly equal absorbance (~ 0.1). The area of the emission spectrum was integrated using the software available in the instrument and the quantum yield was calculated [22] according to the following equation:

$$\Phi_s = \Phi_r \frac{A_s}{A_r} \frac{I_r}{I_s} \frac{\eta_s^2}{\eta_r^2}$$

where Φ_s and Φ_r are the fluorescence quantum yield of the sample and reference, respectively. A_s and A_r are the respective optical densities at the wavelength of excitation, I_s and I_r correspond to the areas under the fluorescence curve; and η_s and η_r are the refractive index values for the sample and reference, respectively. The fluorescence enhancement efficiency (%) was calculated by using the equation $[(F - F_0)/F_0] \cdot 100$ and the corresponding quenching efficiency (%) by $[(F_0 - F)/F_0] \cdot 100$, where F_0 and F are the maximum fluorescence intensities of the complex before exposure and in presence of the analyte, respectively. The Stern-Volmer equation $F_0/F = 1 + K_{sv}[\text{complex}]$ (where F_0 and F are the fluorescence intensities in the absence and presence of the complexes, K_{sv} is Stern-Volmer constant) was used to explain the fluorescence quenching phenomenon [22].

Electrochemical measurements performed under a dry argon atmosphere with a BAS Epsilon electrochemical system. A three-electrode assembly comprising a glassy carbon (for

reduction) or Pt (for oxidation) working electrode, Pt auxiliary electrode and an aqueous Ag/AgCl reference electrode were used. Cyclic voltammetric (CV) measurements were carried out at 298 K using a methanolic solution of complexes (ca. 1 mM) and the concentration of the supporting electrolyte tetraethylammonium perchlorate (TEAM) was maintained at 0.1 M. The potentials reported were referenced against the Ag/AgCl electrode, which under the given experimental conditions gave a value of 0.36 V for the ferrocene/ferrocenium couple.

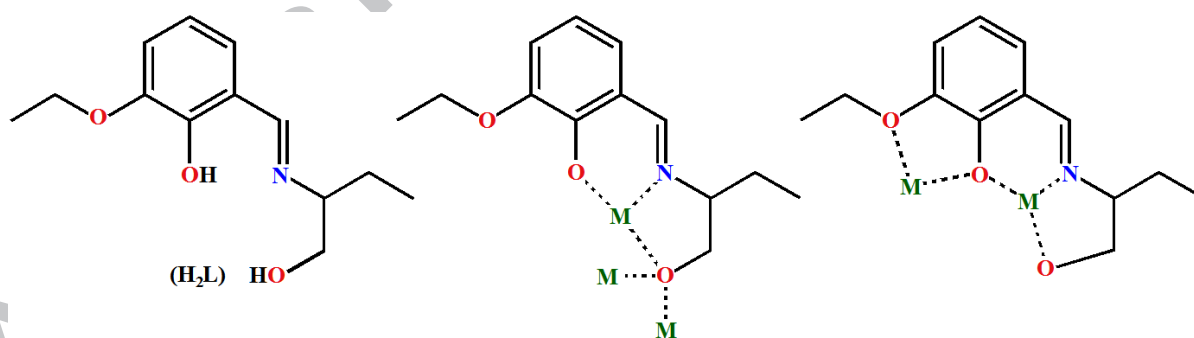
2.2. X-ray crystallography

Data collections for complexes **1** and **2** were carried out at 120 K on an Oxford Diffraction Gemini Ultra diffractometer. Cell refinement, indexing and scaling of the data sets were done with the CrysAlisPro package, Version 1.171.35.10 [23]. The structures were solved using the olex2.solve solution program [24] using the charge flipping algorithm and refined by the full matrix least-squares method based on F^2 with all observed reflections [25]. All the calculations were performed using WinGX [26]. For **1**, three of the four ligands exhibit some form of disorder in the side-chains. This disorder has been modelled in two sets (PART 1 and PART 2) with occupancies of 0.6 and 0.4. One of the perchlorates anions is also disordered in the same ratio. Standard methods to restrain distances and also some ADPs have been employed. These restraints are detailed in the embedded res file and also described explicitly in a textual way. The restraints did not affect the R factors in a negative way. Packing diagrams were obtained with the graphical program Diamond [27]. Crystal data and details of refinements are given in Table 1.

2.3. Synthesis of the ligand and the complexes

2.3.1. Synthesis of 2-ethoxy-6-[(1-hydroxymethyl-propylimino)-methyl]-phenol (H_2L)

A methanolic solution (50 ml) of a 1:1 mixture of 2-aminobutanol (1 mmol, 0.089 g) and 2-hydroxy-3-ethoxybenzaldehyde (1 mmol, 0.166 g) was refluxed for 3 h. The resulting yellow colored solution was cooled to room temperature and a solid yellow compound was obtained after evaporation of the solvent. Re-crystallization of the compound using methanol as the solvent resulted in yellow crystals. The crystalline solid was collected by filtration and dried in air to afford H_2L . Yield: 0.197 g (83%). Anal. calc. for $C_{13}H_{19}NO_3$ (237.29): C, 65.80; H, 8.07; N, 5.90. Found: C, 65.82; H, 8.11; N, 5.22 (%). 1H NMR (400 MHz, $CDCl_3$, δ ppm): 0.796-0.877 (6H, m), 1.414-1.432 (2H, m), 2.586 (1H, s), 3.147-3.190 (1H, m), 3.559-3.683 (2H, m), 4.013-4.048 (2H, m), 4.863 (1H, s), 6.671-6.850 (1H, d; 2H, m), 8.271 (1H, s). ^{13}C NMR ($CDCl_3$, 100 MHz, δ ppm): 153.71 (Ar-C-OH), 165.37 (-CH=N-), 147.96 (C-OEt), 123.08, 118.08, 117.40, 115.29 (Ar-C), 72.14 (-CH₂-OH), 66.28 (=N-CH-), 64.34 (-O-CH₂), 24.98 (-CH₂-), 14.83 (-CH₃ of -OEt), 10.35 (-CH₃).

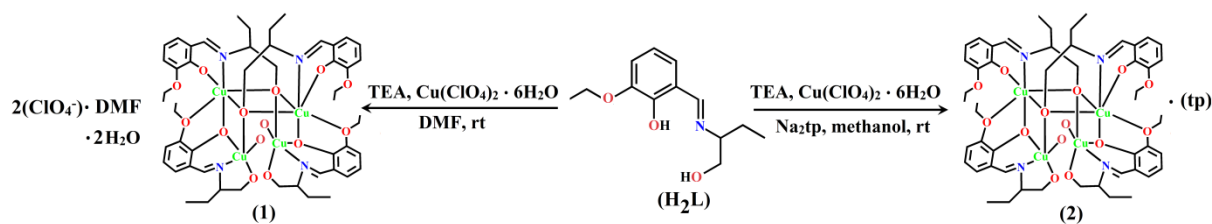


Scheme 1 The structure of H_2L , and its coordination modes in complexes **1** and **2**.

2.3.2. Synthesis of the complexes

Caution! Perchlorate salts of metals with organic ligands are potentially explosive. Only a small amount of the material should be prepared, and it should be handled with care.

The complexes have been synthesized by adopting the procedures given in Scheme 2.



Scheme 2 Synthesis of **1** and **2**.

2.3.2.1. $[Cu_4(L)_2(HL)_2(H_2O)_2] \cdot 2(ClO_4) \cdot 2(H_2O) \cdot DMF$ (**1**)

A methanolic solution (15 ml) of a 1:1 mixture of triethylamine (1 mmol, 0.101 g) and H_2L (1 mmol, 0.237 g) was added dropwise to a methanolic-DMF solution (10 ml) of copper perchlorate hexahydrate (1 mmol, 0.370 g) under stirring conditions. The deep green reaction mixture was stirred for an additional 2 hours and filtered. The filtrate was kept in an open atmosphere for slow evaporation and green single crystals suitable for X-ray diffraction quality were obtained after a few days. Yield: 81%. Anal. calc. for $C_{55}H_{85}Cu_4N_5O_{25}Cl_2$ (1541.33): C, 42.86; H, 5.56; N, 4.54. Found: C, 42.84; H, 5.38; N, 4.53 (%). IR (cm^{-1}): 3430 (vs), 2984 (vw), 1642 (vs), 1550 (vs), 1466 (s), 1413 (vs), 1373 (w), 1244 (vw), 1300 (s), 1078 (s), 882 (vw), 632(vw).

2.3.2.2. $[Cu_4(L)_2(HL)_2(H_2O)_2] \cdot (tp)$ (**2**)

A methanolic solution (15 ml) of a 1:1 mixture of triethylamine (1 mmol, 0.101 g) and H_2L (1 mmol, 0.237 g) was added dropwise to a methanolic solution (10 ml) of copper perchlorate hexahydrate (1 mmol, 0.370 g) under stirring conditions. To the resulting green solution an aqueous solution of sodium terephthalate (1 mmol, 0.21g) was added after 2 hours and stirred for an additional 1 hour, then filtered. The filtrate was kept in air for slow evaporation at room temperature and green single crystals suitable for X-ray diffraction were

obtained after a few days. Yield: 76%. Anal. calc. for $C_{60}H_{78}Cu_4N_4O_{18}$ (1397.46): C, 51.57; H, 5.63; N, 4.01. Found: C, 51.82; H, 5.34; N, 4.07 (%). IR (cm^{-1}): 3435 (vs), 2984 (vw), 1644 (vs), 1551 (vs), 1466 (s), 1414 (vs), 1373 (s), 1300 (s), 1244 (vw), 1079 (s), 882 (vw), 664 (vw).

2.4. Albumin binding studies

Stock solutions of human serum albumin (HSA) and bovine serum albumin (BSA) were prepared in HEPES buffer (pH 7.2). Stock solutions of the complexes were prepared by dissolving the complexes in water. The absorption titration experiments were carried out by keeping the concentration of SA constant (4.75×10^{-5} M for BSA; 3.16×10^{-5} M for HSA), while varying the concentrations of the Cu(II) complexes (0 to 11.2 μ M). The interactions of the compounds with the serum albumins were studied by recording the tryptophan fluorescence of HSA / BSA. To the solutions of serum albumin, the Cu(II) complexes were added at room temperature, and the quenching of emission intensities at 340 nm (λ_{ex} , 280 nm) for BSA and 330 (λ_{ex} , 280 nm) for HSA were recorded after the gradual addition of (20 μ L, 0.3475 mmol) an aqueous solution of the complexes. The Stern-Volmer constant (K_{sv}) and quenching rate constant (k_q) were calculated using the Stern-Volmer equation and the relation $K_{sv} = k_q\tau_0$, where τ_0 is the fluorescence lifetime [28] of the tryptophan residue of serum albumin ($\sim 5 \times 10^{-9}$ s). The binding constant (K_{bin}) and the number of binding sites (n) were calculated using the following Scatchard equation [29], where [complex] is the total concentration of the added complex.

$$\log[(F_0-F)/F] = \log K_{bin} + n \log[\text{complex}]$$

2.5. DNA binding studies

2.5.1. Electronic absorption spectral study

The binding of the complexes with CT-DNA were studied by UV-vis spectroscopy to determine possible DNA-binding modes and binding constants. The UV spectra of the complexes were recorded with a fixed concentration of the complexes (5 μM) in water and varying the concentration of CT-DNA (0-15.48 μM) at room temperature in HEPES buffer (pH = 7.2). Intrinsic binding constants (K_{ib}) of the complexes with CT-DNA were determined using the equation [30]

$$\frac{[\text{DNA}]}{(\varepsilon_a - \varepsilon_f)} = \frac{[\text{DNA}]}{(\varepsilon_b - \varepsilon_f)} + \frac{1}{K_{ib}(\varepsilon_b - \varepsilon_f)}$$

where [DNA] is the concentration of CT-DNA, ε_a is the extinction coefficient value of the complex at a given CT-DNA concentration, ε_f and ε_b are the extinction coefficients of the complex only and when fully bound to CT-DNA, respectively. A plot of $[\text{DNA}]/(\varepsilon_a - \varepsilon_f)$ vs [DNA] gives a straight line with $\frac{1}{(\varepsilon_b - \varepsilon_f)}$ and $\frac{1}{K_{ib}(\varepsilon_b - \varepsilon_f)}$ as the slope and intercept, respectively. From the ratio of the slope to the intercept, the values of K_{ib} were calculated.

2.5.2. Competitive binding fluorescence measurement

Ethidium bromide competitive studies of each compound were carried out, using fluorescence spectroscopy to examine whether the tested compounds **1** and **2** can displace EB from the CT-DNA bound EB system. Aqueous solution of EB bounded CT-DNA (8 μM) solution prepared in HEPES buffer (pH 7.2). In the presence of DNA, ethidium bromide (EB) exhibits fluorescence ($\lambda_{em} = 602 \text{ nm}$, $\lambda_{ex} = 500 \text{ nm}$) enhancement due to its intercalative binding to DNA. Competitive binding of the copper compounds with CT-DNA results in fluorescence quenching due to displacement of EB from CT-DNA. The DNA-intercalating effect of **1** and **2** were studied by gradual addition of the complexes (20 μL , 0.3475 mmol) to

the EB-DNA complex. The fluorescence intensities of EB bounded CT-DNA were recorded with increasing concentrations of the Cu(II) complexes.

3. Results and discussion

3.1. Synthetic aspect

The multisite coordinating ligand H₂L was prepared by a one pot synthesis employing the condensation of 2-amino-1-butanol and 2-hydroxy-3-ethoxybenzaldehyde in methanol under refluxing conditions, and characterized by ¹H and ¹³C NMR spectra (Figs. 1S and 2S). Using H₂L, complexes **1** and **2** were synthesized at room temperature.

3.2. Crystal structures of [Cu₄(L)₂(HL)₂(H₂O)₂]·2(ClO₄)·2(H₂O)·DMF (**1**) and [Cu₄(L)₂(HL)₂(H₂O)₂]·(tp) (**2**)

The molecular structures of **1** and **2** are shown in Figs. 1 and 2. Selected bond lengths and angles are listed in Table 2. Both complexes crystallize in the triclinic system with the P-1 space group. The core structures of both complexes are the same and the only difference is the presence of different lattice molecules (two perchlorate ions and one DMF molecule in **1**, compared to one terephthalate ion in **2**). Both the complexes possess a double open cubane core structure. The tetranuclear cubane core consist of four copper(II) centers, two bideprotonated Schiff base ligands [L²⁻] and two monodeprotonated Schiff base ligands [HL⁻]. Each HL⁻ ligand chelates two copper atoms *via* the μ₂-η¹:η¹:η²-O,O,N,O coordination mode, while the L²⁻ ligand chelates the other two copper centers along with connecting to the previous moieties with a μ₃-alkoxido group, resulting in the μ₃-η¹:η¹:η³-O,N,O coordination mode, while the ethoxy oxygen atoms remain uncoordinated. Fig. 3 and Fig. 3S show a simplified representation of the coordination environment around the four copper centers of

1 and **2**, respectively. For both the complexes, two copper ions are present in a distorted square pyramidal [Cu(1A) and Cu(3A) for **1**; Cu(3) and Cu(4) for **2**] geometry, whereas the other two metal centers are present in a distorted octahedral geometry [Cu(0A) and Cu(2A) for **1**; Cu(1) and Cu(2) for **2**]. The trigonality parameters [31] for five coordinated copper centers are calculated as $(\alpha-\beta)/60$, where α and β are the two largest coordination bond angles. Hence a regular TBP structure with D_{3h} symmetry has $\tau_5 = 1$ and for a regular C_{4v} SP geometry $\tau_5 = 0$. The calculated τ_5 values were 0.252 (Cu(1A)), 0.06 (Cu(3A)) for **1**, and 0.156 (Cu(3)), 0.026 (Cu(4)) for **2**. This result indicates that the copper centers possess distorted square pyramidal geometries. The basal planes of the square pyramid for both the complexes are formed by the imine nitrogen, phenoxide oxygen and alcoholic oxygen atoms of the monodeprotonated HL^- ligand and the μ_3 -alkoxido oxygen atom of the L^{2-} ligand. The coordinated water molecule occupies the apical position of the square pyramid. The basal coordination bond lengths of the square pyramid are between 1.913(19) and 2.017(5) Å for **1** and 1.906(13) and 2.018(8) Å for **2**. The apical bond lengths are somewhat more distant, being at 2.327(5) Å for Cu(1A) and 2.372(6) Å for Cu(3A), respectively in **1**, whereas they are 2.263(7) Å for Cu(3) and 2.271(7) Å for Cu(4) in **2** (Table 2). The coordination environment of other two metal centers [Cu(0A), Cu(2A) for **1** and Cu(1), Cu(2) for **2**] remain distorted octahedral. The basal planes of the octahedron are formed by the imine nitrogen, phenoxido and alkoxido oxygen atoms from one L^{2-} ligand and the μ_2 -phenoxido oxygen atoms of the HL^- ligand, and the axial positions are occupied by ethoxy oxygen atom of the same HL^- ligand and the alkoxido oxygen atom of another L^{2-} ligand. The equatorial bond distances are in the range 1.911(5)-2.016(4) Å for **1** and 1.902(7)-2.021(7) Å for **2**, while relatively larger (due to Jahn-Teller distortion) the axial bond lengths vary from 2.429(5) to 2.582(4) Å for **1** and 2.449(7) to 2.563(8) Å for **2**. The long Cu(1A)-O(7) (3.039 Å) and Cu(3A)-O(1AA) (2.991 Å) distances in **1** and Cu(3)-O(10) (3.003 Å) and Cu(4)-O(2)

(2.959 Å) for **2** are responsible for the formation of the double open cubane core structure. The copper atoms are located at the vertices of a distorted tetrahedron with edge dimension ranges of 3.199(12)-3.888(12) Å for **1** and 3.147(23) -3.891(20) Å for **2** (Figs. 4S and 5S).

Based on the Cu...Cu distances within Cu₄O₄ cubane cores, Alvarez et al. classify [32] copper cubanes into three types: (i) (2+4), where the Cu...Cu distances are two short and four long; (ii) (4+2), where the Cu...Cu distances are two long and four short; and (iii) (6+0), where the six Cu...Cu distances of the Cu₄O₄ cubane core are similar [32c]. However in complex **1**, the Cu...Cu distances are 3.199(12), 3.250(10), 3.207(12), 3.406(12), 3.434(9) and 3.888(12) Å, and in **2**, the Cu...Cu distances are 3.147(23), 3.193(20), 3.891(20), 3.346(15), 3.351(17) and 3.309(18) Å. The Cu...Cu distances in **1** and **2** indicate that the Cu₄O₄ cubane cores of these complexes do not belong to any of the above categories as proposed by Alvarez et al.

The lattice terephthalate ions in complex **2** form 1D supramolecular chains through four different types hydrogen bonding interactions, [O(3)-H(3)...O(17) = 1.73, O(5)-H(5B)...O(16) = 1.98, O(12)-H(12)...O(15) = 1.84 and O(13)-H(13A)...O(14) = 1.78 Å], with the cubane units (Fig. 4).

3.3. Electronic absorption and fluorescence spectra of the complexes

The electronic absorption spectra of the complexes show (Fig. 9S) significant transitions at 231 nm ($\epsilon \sim 8.82 \times 10^4$ litre mole⁻¹ cm⁻¹ for **1** and 6.14×10^4 litre mole⁻¹ cm⁻¹ for **2**), 276 nm ($\epsilon \sim 4.62 \times 10^4$ litre mole⁻¹ cm⁻¹ for **1** and 2.94×10^4 litre mole⁻¹ cm⁻¹ for **2**) and 370 nm ($\epsilon \sim 1.3 \times 10^4$ litre mole⁻¹ cm⁻¹ for **1** and 8.0×10^3 litre mole⁻¹ cm⁻¹ for **2**). The results of the study on the luminescence properties are summarized in Table 3. Both the complexes exhibit red shifted emissions. On excitation at 370 nm, complex **1** exhibits a sharp emission band at 430 nm and two weak shoulders at 458 and 572 nm, whereas for complex **2**

upon excitation at 370 nm it exhibits a sharp emission band at 453 nm and a weak shoulder at 564 nm. The positions of the emission bands remain unchanged when λ_{ex} is varied between ($\lambda_{\text{ex}} - 10$) and ($\lambda_{\text{ex}} + 10$) nm (Fig. 10S). The calculated values of the fluorescence quantum yields (Φ_s) are 0.41 and 0.40 for **1** and **2**, respectively.

3.4. ESI mass spectroscopy

The ESI mass spectra of the complexes were recorded using their methanolic solutions, which were prepared 24 h before the mass spectral study. ESI-mass spectra (Figs. 14S, 15S) of the complexes show peaks at $m/z = 1231.98$ and 1231.31 for complexes **1** and **2**, respectively. The mass spectral peaks correspond to the cationic unit $[\text{Cu}_4(\text{L})_4(\text{H}_2\text{O})_2]^{+}$ (calc. $m/z = 1231.33$ for both **1** and **2**). This result indicates that tetranuclear copper clusters are stable in methanolic solution for 24 h.

3.5. Protein binding studies

A study of the interaction of the complexes with serum albumins has been performed using Uv-vis absorption and fluorescence spectroscopic techniques.

3.5.1. Absorption spectral studies

The changes in the electronic absorption spectra of BSA (3 ml, 0.475 μM aqueous solution) and HSA (3 ml, 0.316 μM aqueous solution) after the gradual addition (20 μL , 0.3475 mmol) of the complex solutions (at pH 7.2 using HEPPEs buffer) at a temperature of 300 K are shown in Figs. 11S and 12S. The absorption intensities for both BSA and HSA were enhanced with a little blue shift (2 nm for **1**; 3 nm for **2**). The shift of the electronic spectral band revealed the existence of a static interaction between the SAs and the

complexes [33]. The apparent association constants (K_a) were calculated from the $1/[\text{complex}]$ vs $1/(A_{\text{abs}}-A_0)$ plot (Fig. 5) using the following equation:

$$\frac{1}{(A_{\text{obs}} - A_0)} = \frac{1}{(A_c - A_0)} + \frac{1}{K_a(A_c - A_0)[\text{complex}]}$$

The values of the apparent association constant (K_a) are depicted in Table 4. The order of the association constant values are comparable to those reported for copper(II)-Schiff base complexes [34].

3.5.2. Fluorescence spectroscopic studies

The changes in the emission spectra of the serum albumins upon addition of increasing concentrations (0-11.2 μM) of complexes are shown in Fig. 6. The fluorescence intensity of BSA at ~ 340 nm was quenched with a small blue shift (52.80%, 4 nm for **1**; 46.81%, 3 nm for **2**). The 330 nm emission band of HSA was also quenched with a blue shift (45.47%, 4 nm for **1**; 36.90%, 4 nm for **2**). The blue shift primarily arises due to the presence of the active site of the protein in a hydrophobic environment [35]. From this observation it is clear that some interaction is taking place between the complexes and SAs. From the Stern-Volmer equation [22] a linear relationship was obtained for the titration of the serum albumins using the complexes as a quencher (inset of Fig. 6). The calculated values of the Stern-Volmer quenching constant (K_{SV}) and the quenching rate constant (K_q) (Table 4) for BSA binding are $K_{SV} = 9.51 (\pm 0.09) \times 10^4 \text{ M}^{-1}$, $K_q = 1.90 (\pm 0.09) \times 10^{13} \text{ M}^{-1}\text{S}^{-1}$ for **1** and $K_{SV} = 7.99 (\pm 0.01) \times 10^4 \text{ M}^{-1}$, $K_q = 1.59 (\pm 0.01) \times 10^{13} \text{ M}^{-1}\text{S}^{-1}$ for **2**. For HSA binding the values are $K_{SV} = 7.45 (\pm 0.07) \times 10^4 \text{ M}^{-1}$, $K_q = 1.49 (\pm 0.07) \times 10^{13} \text{ M}^{-1}\text{S}^{-1}$ for **1** and $K_{SV} = 5.12 (\pm 0.06) \times 10^4 \text{ M}^{-1}$, $K_q = 1.02 (\pm 0.06) \times 10^{13} \text{ M}^{-1}\text{S}^{-1}$ for **2**. The magnitudes of the K_{SV} values indicate that both the complexes have a good fluorescence quenching ability.

The UV-vis absorption spectra of the SAs show a noticeable change in the presence of the complexes. This indicates the presence of a static interaction between the SAs and complexes

1 and **2**. To have a deep insight into the quenching sequence, the equilibrium binding constant (K_{bin}) and number of binding sites (n) were also evaluated from the plot of $\log [(F_0 - F)/F]$ versus $\log [\text{complex}]$ (Fig. 7) using the Scatchard equation [29]. The binding constants (K_{bin}) and the number of binding sites per albumin (n) for the complexes are given in Table 4. The calculated value of n is around 1 for all the complexes, indicating the existence of just a single binding site in the SAs for the complexes.

3.6. Interaction with Calf-Thymus DNA

Metal complexes bind to double-stranded DNA via covalent or non-covalent interactions. Non-covalent interactions with DNA involve three binding modes: intercalative binding, groove binding and electrostatic interactions [36]. Here the interactions of the complexes with CT-DNA were studied with UV-vis absorption and ethidium bromide (EB) displacement studies.

3.6.1. UV-vis absorption spectral studies

The absorption spectra of the complexes in the absence and presence of CT-DNA are shown in Fig. 8. Addition of increasing amounts (0-15.48 μM) of CT-DNA results in an increase in the absorption intensity of the complexes and in a significant shift in the band position. For **1**, the absorption bands at 231, 276 and 370 nm showed hyperchromism with 4 nm red, 8 nm blue and 5 nm red shifts, respectively. For **2**, the bands at 231, 276 and 370 nm showed hyperchromism with 6 nm red, 13 nm blue and 4 nm red shifts, respectively. From the plots of $[\text{DNA}] / (\epsilon_a - \epsilon_f)$ versus $[\text{DNA}]$ (inset of Fig. 8), linear relationships were obtained, and the intrinsic binding constants (K_{ib}) were calculated from the ratio of the slope and the intercept. The calculated values of K_{ib} are $1.25 (\pm 0.22) \times 10^4$ and $8.77 (\pm 0.10) \times 10^3 \text{ M}^{-1}$ (Table 5) for **1** and **2** respectively. These results indicate that both the new copper complexes bind to the CT-DNA helix.

3.6.2. Competitive binding between ethidium bromide and the complexes

Absorption titration studies indicated that **1** and **2** effectively bind with CT-DNA. The nature of the binding between the complexes and CT-DNA was also studied adopting ethidium bromide (EB) displacement experiments. EB is a planar cationic dye and it is one of the most sensitive fluorescence probes which can bind to DNA through intercalation [37]. The changes of the emission spectra of EB bonded CT-DNA with increasing concentrations of the complexes are shown in Fig. 9. Due to the displacement of EB from the CT-DNA sequence by the complexes, the fluorescence intensity decreases as the number of binding sites on the DNA available for EB are also reduced. It is of note that **1** and **2** do not show any significant fluorescence when excited at 500 nm in the presence of CT-DNA. Furthermore the addition of the complexes to a solution containing only EB do not show any quenching of the free EB fluorescence.

On gradual addition of the complexes (20 μ L, 0.3475 μ M) to an EB bonded CT-DNA solution, the quenching of the emission of EB bounded CT-DNA was observed. The 602 nm emission band exhibited hypochromism up to 63.13% (for **1**) and 52.53% (for **2**) of the initial fluorescence intensity. The observed decrease in fluorescence intensity is due to displacement of EB from CT-DNA binding sites by the complexes [38]. The Stern-Volmer plots (inset of Fig. 9) for these fluorescence titrations show straight lines ($R = 0.9796, 0.9963$). The K_{sv} values have been derived from the slope of F_0/F vs [complex] plots, and the values are $1.483 (\pm 0.11) \times 10^5$ (for **1**) and $9.78 (\pm 0.08) \times 10^4 \text{ M}^{-1}$ (for **2**). The apparent DNA binding constant (K_{app}) values were calculated using the equation [33a]

$$K_{EB}[EB] = K_{app}[\text{complex}]$$

where the complex concentration is the value at a 50% reduction in the fluorescence intensity of EB, K_{EB} ($1.0 \times 10^7 \text{ M}^{-1}$) is the DNA binding constant of EB, [EB] is the

concentration of EB (8 μM). The K_{app} values were found to be 8.86×10^5 and 7.14×10^5 for **1** and **2**, respectively and these results are given in Table 5. From these observed data, it is seen that both the complexes have comparable binding affinities. A comparison (Table 6) of the kinetic parameters of the CT-DNA interaction of the present compounds with reported tetranuclear cubane core (Cu_4O_4) complexes, $[\text{Cu}_4(\text{L}^1)_4] [3\text{g}] (\text{H}_2\text{L}^1$; Schiff base of 1-amino-2-propanol and salicylaldehyde) and $\{[\text{Cu}_4(\mu\text{-L}^2)_2(\mu_{1,1,3,3}\text{-O}_2\text{CH})](\text{OH})\cdot 6\text{H}_2\text{O}\} [3\text{h}] (\text{H}_3\text{L}^2$; 1,3-bis[3-aza-3-(1-methyl-3-oxobut-1-enyl)prop-3-en-1-yl]-2-(2-hydroxyphenyl)-1,3-imidazolidine) show that **1** and **2** have comparable binding affinities with the reported compounds.

3.7. Redox properties of the complexes

The electrochemical behavior of the complexes was investigated in methanol solution by cyclic voltammetry in the potential range between 0.3 and 0.7 V. The voltammetric data are collected in Table 3 and the voltammograms are displayed in Fig. 10. The cyclic voltammograms show irreversible oxidation processes at 0.51 and 0.48 V for **1** and **2**, respectively.

4. Conclusion

In summary, we have presented here the synthesis, crystal structure, DNA and protein binding studies of two 2-ethoxy-6-[(1-hydroxymethyl-propylimino)-methyl]-phenol (H_2L) ligand based copper(II) complexes (**1** and **2**). The X-ray structural analysis shows that in both complexes the H_2L ligand is present in its mono (HL^-) and dianionic (L^{2-}) forms with the $\mu_2\text{-}\eta^1:\eta^1:\eta^1:\eta^2\text{-O,O,N,O}$ and $\mu_3\text{-}\eta^1:\eta^1:\eta^3\text{-O,N,O}$ coordination modes, respectively. Both the

complexes possess a double open [Cu₄O₄] cubane core structure and the only difference is the presence of lattice solvents and anions. Supramolecular C-H... π interactions result in the 2D and 3D supramolecular architectures of **1** and **2**, respectively. The CT-DNA and protein binding of the compounds were investigated using electronic absorption and emission spectroscopic techniques. The compounds bind effectively with CT-DNA in the order 10⁴ M⁻¹ through a non-intercalative interaction. A fluorescence spectroscopic study evidences that the interactions of **1** and **2** with serum albumins occur through a ground state association process.

Acknowledgement

The authors gratefully acknowledge the financial assistance given by the CSIR, Government of India, to Dr. Subal Chandra Manna (Project No. 01 (2743)/13/EMR-II). Dr. S. C. Manna thanks UGC-SAP, DST-FIST New Delhi, USIC (VU) for instrumental facilities and Vidyasagar University for infrastructural facilities.

Appendix A. Supplementary data

CCDC 1544798 and 1544799 contain the supplementary crystallographic data for **1** and **2** respectively. These data can be obtained free of charge via <http://www.ccdc.cam.ac.uk/conts/retrieving.html>, or from the Cambridge Crystallographic Data Centre, 12 Union Road, Cambridge CB2 1EZ, UK; fax: (+44) 1223-336-033; or e-mail: deposit@ccdc.cam.ac.uk. Tables for hydrogen interactions, C-H... π interactions; figures of NMR, FT-IR and electronic spectra and crystal structure data are provided as supporting information.

References

[1] a) D. Gatteschi, R. Sessoli, *Angew. Chem. Int. Ed.*, 42 (2003) 268-297; b) R.E.P. Winpenny, *Adv. Inorg. Chem.*, 52 (2001) 1-11.

[2] a) R.H. Holm, P. Kennepohl, E.I. Solomon, *Chem. Rev.*, 96 (1996) 2239-2314; b) R. Huber, *Angew. Chem. Int. Ed.*, 28 (1989) 848-869; c) E.I. Solomon, R.K. Szilagy, S. De Beer George, L. Basumallick, *Chem. Rev.*, 104 (2004) 419-458; d) L. Tjioe, A. Meininger, T. Joshi, L. Spiccia, B. Graham, *Inorg. Chem.*, 50 (2011) 4327-4339; e) S.S. Bhat, A.A. Kumbhar, H. Heptullah, A.A. Khan, V.V. Gobre, S.P. Gejji, V.G. Puranik, *Inorg. Chem.*, 50 (2011) 545-558.

[3] a) R.H. Bode, W.L. Driessen, F.B. Hulsbergen, J. Reedijk, A.L. Spek, *Eur. J. Inorg. Chem.*, (1999) 505-507; b) M. Murugesu, R. Clerac, B. Pilawa, A. Mandel, C.E. Anson, A.K. Powell, *Inorg. Chim. Acta*, 337 (2002) 328-336; c) R. Acevedo-Chavez, M.E. Costas, S. Bernes, G. Medina, L. Gasque, *J. Chem. Soc., Dalton Trans.*, (2002) 2553-2558; d) Z.Q. Xu, L.K. Thompson, D.O. Miller, *Chem. Commun.*, (2001) 1170-1171; e) B. Graham, M.T.W. Hearn, P.C. Junk, C.M. Kepert, F.E. Mabbs, B. Moubaraki, K.S. Murray, L. Spiccia, *Inorg. Chem.*, 40 (2001) 1536-1543; f) J. Sletten, A. Sørensen, M. Julve, Y. Journaux, *Inorg. Chem.*, 29 (1990) 5054-5058; g) R. Vafazadeh, A. C. Willis, *J. Coord. Chem.*, 68 (2015) 2240-2252; h) T.S. Mahapatra, A. Roy, S. Chaudhury, S. Dasgupta, S.L. Shrivastava, V. Bertolasi, D. Ray, *Eur. J. Inorg. Chem.*, (2017) 769-779; i) M. Niu, Z. Li, H. Li, X. Li, J. Dou, S. Wang, *RSC Adv.*, 5 (2015) 37085-37095; j) M. Usman, F. Arjmand, R.A. Khan, A. Alsalme, M. Ahmad, M.S. Bishwas, S. Tabassum, *Inorg. Chim. Acta*, 473 (2018) 121-132.

[4]a) C. Aronica, Y. Chumakov, E. Jeanneau, D. Luneau, P. Neugebauer, A.-L. Barra, B. Gillon, A. Goujon, A. Cousson, J. Tercero, E. Ruiz, *Chem.-Eur. J.*, 14 (2008) 9540-9548; b) B. Sarkar, M. Sinha Ray, Y.-Z. Li, Y. Song, A. Figuerola, E. Ruiz, J. Cirera, J. Cano, A. Ghosh, *Chem.-Eur. J.*, 13 (2007) 9297-9309; (c) A. Mukherjee, R. Raghunathan, M.K. Saha, M. Nethaji, S. Ramasesha, A.R. Chakravarty, *Chem.-Eur. J.*, 11 (2005) 3087-3096; (d) S.C.

Manna, S. Manna, A. Paul, E. Zangrando, A. Figuerola, S. Dolai, K. Das, *ChemistrySelect*, 2 (2017) 3317-3322.

[5] a) A.M. Kirillov, M.V. Kirillova, A.J.L. Pombeiro, *Adv. Inorg. Chem.*, 65 (2013) 1-31; b) S.E. Allen, R.R. Walvoord, R. Padilla-Salinas, M.C. Kozlowski, *Chem. Rev.*, 113 (2013) 6234-6458; c) A. Sakakura, K. Ishihara, *Chem. Soc. Rev.*, 40 (2011) 163-172; d) S. Banerjee, D.P. Kumar, S. Bandyopadhyay, N.N. Adarsh, P. Dastidar, *Cryst. Growth Des.*, 12 (2012) 5546-5554; e) C. Di Nicola, F. Garau, M. Gazzano, M.F.C. Guedes da Silva, A. Lanza, M. Monari, F. Nestola, L. Pandolfo, C. Pettinari, A.J.L. Pombeiro, *Cryst. Growth Des.*, 12 (2012) 2890-2901.

[6] R. Than, A.A. Feldmann, B. Krebs, *Coord. Chem. Rev.*, 182 (1999) 211-241.

[7] a) J. Tang, J.S. Costa, A. Pevec, B. Kozlevčar, C. Massera, O. Roubeau, I. Mutikainen, U. Turpeinen, P. Gamez, J. Reedijk, *Cryst. Growth Des.*, 8 (2008) 1005-1012; b) A. Karmakar, C.L. Oliver, S. Roy, L. Öhrström, *Dalton Trans.*, 44 (2015) 10156-10165.

[8] S.S.P. Dias, M.V. Kirillova, V. Andre[^], J. Kłak, A.M. Kirillov, *Inorg. Chem.*, 54 (2015) 5204-5212.

[9] a) Y. Song, C. Massera, O. Roubeau, P. Gamez, A. Maria, M. Lanfredi, J. Reedijk, *Inorg. Chem.*, 43 (2004) 6842-6847; b) A. Paul, V. Bertolasi, A. Figuerola, S.C. Manna, *J. Solid State Chem.*, 249 (2017) 29-38.

[10] a) N. Lah, I. Leban, R. Clérac, *Eur. J. Inorg. Chem.*, (2006) 4888-4894; b) H. Liu, H. Wang, H. Wu, D. Niu, *J. Coord. Chem.*, 58 (2005) 1345-1349.

[11] Y. Yoshikawa, H. Yasui, *Cur. Top. Med. Chem.*, 12 (2012) 210-218.

[12] a) M.S. Islas, J.J.M. Medina, L.L.L. Tézvez, T. Rojo, L. Lezama, M.G. Merino, L. Calleros, M.A. Cortes, M.R. Puyol, G.A. Echeverría, O.E. Piro, E.G. Ferrer, P.A.M.

Williams, *Inorg. Chem.*, 53 (2014) 5724-5437; b) A. Wojciechowska, A. Gaĝor, W. Zierkiewicz, A. Jarzab, A. Dylong, M. Duczmal, *RSC Adv.*, 5 (2015) 36295-36306.

[13] a) A.M. Abu-Dief, I.M.A. Mohamed, *Beni-Suef University Journal of Basic and Applied Sciences*, 4 (2015)119-133; b) F. Rahaman, B.H.M. Mruthyunjayaswamy, *Complex Met.*, 1 (2014) 88-95.

[14] S. Muche, I. Levacheva, O. Samsonova, L. Pham, G. Christou, U. Bakowsky, M. Hołyńska, *Inorg. Chem.*, 53 (2014) 7642-7649.

[15] D.-D. Yin, Y.-L. Jiang, L. Shan, *Chinese J. Chem.*, 19 (2001) 1136-1140.

[16] J. Vanĝo, O. Švajlenová, E. Raĝanská, J. Muselík, J. Valentová, *J. Trace Elem. Med. Biol.*, 18 (2004) 155-161.

[17] a) J. Vanĝo, J. Marek, Z. Trávníĝek, E. Raĝanská, J. Muselík, O. Švajlenová, *J. Inorg. Biochem.*, 102 (2008) 595-605.

[18] a) A. Nori, J. Kopecek, *Adv. Drug Delivery Rev.*, 57 (2005) 609-636; b) Y. Xie, G.G. Miller, S.A. Cubitt, K.J. Soderlind, M.J. Allalunis-Turner, J.W. Lown, *Anti-Cancer Drug Des.*, 12 (1997) 169-179; c) M. Shi, K. Ho, A. Keating, M.S. Shoichet, *Adv. Funct. Mater.*, 19 (2009) 1689-1696; d) W.O. Foye, *Cancer Chemotherapeutic Agents*, American Chemical Society, Washington, DC, 1995.

[19] a) B. Rosenberg, L. Vam Camp, J.E. Trosko, V.H. Mansour, *Nature*, 222 (1969) 385-386; b) D. Senthil Raja, N.S.P. Bhuvanesh, K. Natarajan, *Dalton Trans.*, 41 (2012) 4365-4377; c) X. Qiao, Z.Y. Ma, C.Z. Xie, F. Xue, Y.W. Zhang, J.Y. Xu, Z.Y. Qiang, J.S. Lou, G.J. Chen, S.P. Yan, *J. Inorg. Biochem.*, 105 (2011) 728-737; d) P.J. Bednarski, F.S. Mackay, P.J. Sadler, *Adv. Anticancer Agents Med. Chem.*, 7 (2007) 75-93.

[20] J. Costa Pessoa, I. Tomaz, *Curr. Med. Chem.*, 17 (2010) 3701-3778.

- [21] D.D. Perrin, W.L.F. Armarego, D.R. Perrin, Purification of Laboratory Chemicals; Pergamon Press: Oxford, U.K., 1980.
- [22] J.R. Lakowicz, Principles of Fluorescence Spectroscopy, Third Edition, Springer, New York, USA, 2006.
- [23] CrysAlis PRO, Agilent Technologies Ltd, Yarnton, 2010.
- [24] O.V. Dolomanov, L.J. Bourhis, R.J. Gildea, J.A.K. Howard, H. Puschmann, J. Appl. Crystallogr., 42 (2009) 339-341.
- [25] G.M. Sheldrick, ActaCrystallogr., A64 (2008) 112-122.
- [26] L.J. Farrugia, J. Appl. Crystallogr., 32 (1999) 837-838.
- [27] K. Brandenburg, DIAMOND (Version 3.2i), Crystal Impact GbR, Bonn, Germany, 1999.
- [28] P. Smoleński, C. Pettinari, F. Marchetti, M. Fátima C. Guedes da Silva, G. Lupidi, G.V. B. Patzmay, D. Petrelli, L.A. Vitali, A.J.L. Pombeiro, Inorg. Chem., 54 (2015) 434-440.
- [29] a) J.R. Lakowicz, Fluorescence Quenching: Theory and applications, Principles of Fluorescence Spectroscopy, Kluwer Academic / Plenum Publishers, New York, 1999, pp. 53-127; b) X.-Z. Feng, Z. Lin, L.-J. Yang, C. Wang, C.-L. Bai, Talanta, 47 (1998) 1223-1229.
- [30] A. Wolfe, G.H. Shimer, T. Mehan, Biochemistry, 26 (1987) 6392-6396.
- [31] A.W. Addison, T.N. Rao, J. Reedijk, J.V. Rijn, G.C. Verschoor, J. Chem. Soc., Dalton Trans., (1984) 1349-1356.
- [32] a) J. Tercero, E. Ruiz, S. Alvarez, A. Rodríguez-Forteza, P. Alemany, J. Mater. Chem., 16 (2006) 2729-2735; b) E. Ruiz, S. Alvarez, A. Rodríguez-Forteza, P. Alemany, Y. Pouillon, C. Massobrio, J.S. Miller, M. Drillon Eds., Electronic Structure and Magnetic Behavior in Polynuclear Transition-Metal Compounds, vol. 2, Wiley-VCH, Weinheim, Germany, 2001; c) E. Ruiz, A. Rodríguez-Forteza, P. Alemany, S. Alvarez, Polyhedron, 20 (2001) 1323-1327.

- [33] a) E. Ramachandran, D.S. Raja, N.P. Rath, K. Natarajan, *Inorg. Chem.*, 52 (2013) 1504-1514; b) D. Senthil Raja, N.S.P. Bhuvanesh, K. Natarajan, *Inorg. Chem.*, 50 (2011) 12852-12866.
- [34] a) A. Paul, A. Figuerola, V. Bertolasi, S.C. Manna, *Polyhedron*, 119 (2016) 460-470; b) X.-Q. Zhou, Q. Sun, L. Jiang, S.-T. Li, W. Gu, J.-L. Tian, X. Liu, S.-P. Yan, *Dalton Trans.*, 44 (2015) 9516-9527; c) W.-J. Lian, X.-T. Wang, C.-Z. Xie, H. Tian, X.-Q. Song, H.-T. Pan, X. Qiao, J.-Y. Xu, *Dalton Trans.*, 45 (2016) 9073-9087; d) K.M. Vyas, R.N. Jadeja, D. Patel, R.V. Devkar, V.K. Gupta, *Polyhedron*, 80 (2014) 20-33; e) K. Jeyalakshmi, Y. Arun, N.S.P. Bhuvanesh, P.T. Perumal, A. Sreekanth, R. Karvembu, *Inorg. Chem. Front.*, 2 (2015) 780-798.
- [35] a) P. Krishnamoorthy, P. Sathyadevi, A.H. Cowley, R. Butorac, N. Dharmaraj, *Eur. J. Med. Chem.*, 46 (2011) 3376-3387; b) P. Sathyadevi, P. Krishnamoorthy, R. Butorac, A.H. Cowley, N.S.P. Bhuvanesh, N. Dharmaraj, *Dalton Trans.*, 40 (2011) 9690-9702; c) P. Krishnamoorthy, P. Sathyadevi, A.H. Cowley, R. Butorac, N. Dharmaraj, *Dalton Trans.*, 41 (2012) 6842-6854; d) D. Senthil Raja, N.S.P. Bhuvanesh, K. Natarajan, *Eur. J. Med. Chem.*, 46 (2011) 4584-4594.
- [36] a) F. Dimiza, S. Fountoulaki, A.N. Papadopoulos, C.A. Kontogiorgis, V. Tangoulis, C.P. Rapatopoulou, V. Psycharis, A. Terzis, D.P. Kessissoglou, G. Psomas, *Dalton Trans.*, 40 (2011) 8555-8568; b) S. Tsiliou, L. Kefala, F. Perdih, I. Turel, D.P. Kessissoglou, G. Psomas, *Eur. J. Med. Chem.*, 48 (2012) 132-142; c) A. Tarushi, X. Totta, C.P. Rapatopoulou, V. Psycharis, G. Psomas, D.P. Kessissoglou, *Dalton Trans.*, 41 (2012) 7082-7091; d) A. Tarushi, X. Totta, A. Papadopoulos, J. Kijun, I. Turel, D.P. Kessissoglou, G. Psomas, *Eur. J. Med. Chem.*, 74 (2014) 187-198; e) M. Zampakou, N. Rizeq, V. Tangoulis, A.N. Papadopoulos, F. Perdih, I. Turel, G. Psomas, *Inorg. Chem.*, 53 (2014) 2040-2052.

[37] a) F.J. Meyer-Almes, D. Porschke, *Biochemistry*, 32 (1993) 4246-4253; b) G.M. Howe, K. C. Wu, W. R. Bauer, *Biochemistry*, 19 (1976) 339-347.

[38] a) P. Kumar, S. Gorai, M. Kumar, B. Mondal, D. Manna, *Dalton Trans.*, 41 (2012) 7573-7581; b) M.A. Kostianen, J.G. Hardy, D.K. Smith, *Angew. Chem. Int. ed.*, 44 (2005) 2556-2559.

Table 1 Crystal data and structure refinement of complexes **1** and **2**.

Complex	1	2
Empirical formula	C ₅₅ H ₈₅ Cu ₄ N ₅ O ₂₅ Cl ₂	C ₆₀ H ₇₈ Cu ₄ N ₄ O ₁₈
Formula mass, g mol ⁻¹	1541.33	1397.46
Crystal system	Triclinic	Triclinic
Space group	<i>P</i> -1	<i>P</i> -1
<i>a</i> , Å	11.6628(6)	13.1269(12)
<i>b</i> , Å	14.0257(7)	15.7400(15)
<i>c</i> , Å	20.9237(6)	16.5893(11)
α , deg	93.892(3)	93.042(7)
β , deg	98.319(3)	104.161(7)
γ , deg	107.142(4)	110.732(9)
<i>V</i> , Å ³	3214.0(3)	3071.2(5)
<i>Z</i>	2	2
<i>D</i> _(calcd) , g cm ⁻³	1.577	1.509
μ (Mo-K α), mm ⁻¹	1.472	1.441
<i>F</i> (000)	1582	1448
Theta range, deg	1.9, 25.0	1.8, 25.0
No. of collected data	47359	29770
No. of unique data	11315	10798
<i>R</i> _{int}	0.085	0.093
Observed reflns [<i>I</i> > 2 σ (<i>I</i>)]	8532	5375
Goodness of fit (<i>F</i> ²)	1.073	1.020
Parameters refined	11315, 1041	10798, 783
<i>R</i> 1, <i>wR</i> 2 (<i>I</i> > 2 σ (<i>I</i>)) ^[a]	0.0727, 0.1732	0.0918, 0.2707
Residuals, e Å ⁻³	-1.38, 1.53	-0.59, 0.88

$$^{[a]}R1(F_o) = \sum ||F_o| - |F_c|| / \sum |F_o|, wR2(F_o^2) = [\sum w (F_o^2 - F_c^2)^2 / \sum w (F_o^2)^2]^{1/2}$$

Table 2 Coordination bond lengths (Å) and angles (°) for complexes **1** and **2**.

	1		2
Bond lengths			
Cu(0A)-O(2AA)	1.912(5)	Cu(1)-O(1)	2.449(7)
Cu(0A)-O(6)	2.433(4)	Cu(1)-O(0AA)	1.953(7)
Cu(0A)-O(7)	1.991(4)	Cu(1)-O(6)	1.902(7)
Cu(0A)-O(8)	1.963(5)	Cu(1)-O(10)	2.005(8)
Cu(0A)-O(9)	2.582(4)	Cu(1)-O(11)	2.563(8)
Cu(0A)-N(5)	1.940(5)	Cu(1)-N(3)	1.943(12)
Cu(1A)-O(1AA)	1.944(5)	Cu(2)-O(1)	1.941(7)
Cu(1A)-O(8)	1.918(4)	Cu(2)-O(0AA)	2.500(8)
Cu(1A)-O(0AA)	2.327(5)	Cu(2)-O(2)	2.021(7)
Cu(1A)-O(7AA)	2.017(5)	Cu(2)-O(4)	2.528(8)
Cu(1A)-N(4)	1.913(19)	Cu(2)-O(8)	1.912(7)
Cu(2A)-O(1AA)	2.016(4)	Cu(2)-N(4)	1.940(9)
Cu(2A)-O(5AA)	1.911(5)	Cu(3)-O(0AA)	1.919(7)
Cu(2A)-O(4AA)	2.429(5)	Cu(3)-O(2)	1.979(7)
Cu(2A)-O(8)	2.520(4)	Cu(3)-O(3)	2.018(8)
Cu(2A)-O(9)	1.955(5)	Cu(3)-O(5)	2.263(7)
Cu(2A)-N(6)	1.940(5)	Cu(3)-N(1)	1.934(10)
Cu(3A)-O(4)	2.372(6)	Cu(4)-O(1)	1.921(7)
Cu(3A)-O(7)	1.942(5)	Cu(4)-O(10)	1.962(8)
Cu(3A)-O(9)	1.917(4)	Cu(4)-O(12)	1.973(10)
Cu(3A)-O(11)	2.009(6)	Cu(4)-O(13)	2.271(7)
Cu(3A)-N(2)	1.983(18)	Cu(4)-N(5)	1.906(13)
Bond angles			
Cu(0A)-O(7)-Cu(3A)	109.3(2)	Cu(1)-O(1)-Cu(2)	97.1(3)
Cu(0A)-O(8)-Cu(2A)	92.06(18)	Cu(1)-O(1)-Cu(4)	91.3(2)
Cu(1A)-O(8)-Cu(2A)	91.21(16)	Cu(2)-O(1)-Cu(4)	120.1(3)
Cu(0A)-O(8)-Cu(1A)	124.5(2)	Cu(1)-O(0AA)-Cu(2)	95.2(3)
Cu(2A)-O(9)-Cu(3A)	123.2(2)	Cu(1)-O(0AA)-Cu(3)	119.9(4)
Cu(0A)-O(9)-Cu(2A)	90.41(18)	Cu(2)-O(0AA)-Cu(3)	91.6(3)
Cu(0A)-O(9)-Cu(3A)	89.66(16)	Cu(2)-O(2)-Cu(3)	106.0(4)

Table 3 Electronic absorption and emission spectra of **1** and **2**.

	UV-vis ^a λ_{\max} ; ϵ ($M^{-1}cm^{-1}$)	Emission (nm)	$\Delta\nu^c$, (nm)	Φ_s	E_{Ox}^d (V), i_{ac}^e (μA)	FT-IR, ν^g (cm^{-1})
1	231 (8.82 $\times 10^4$), 276 (4.62 $\times 10^4$), 370 (1.3 $\times 10^4$)	430	60	0.41	0.514, -7.109	3430(br) [v(O-H)], 2984 [v(C-H)], 1642(vs) [v(H-O- H)bending], 1550 [v(C=N)]
2	231 (6.14 $\times 10^4$), 276 (2.94 $\times 10^4$), 370 (8.0 $\times 10^3$)	453	83	0.40	0.485, -2.334	3435(br) [v(O-H)], 2984 [v(C-H)], 1644 [v _{as} (OCO)], 1551 [v(C=N)], 1414 [v _s (OCO)]

Bold number indicates the excitation wavelength. [a] Wavelength in nanometers, [b] Molar extinction coefficient in $M^{-1}cm^{-1}$ in methanol solvent. [c] Stoke shift, [d] Methanol solution (supporting electrolyte NEt_4ClO_4 , working electrode glassy carbon, reference electrode $Ag/AgCl$, scan rate 100 mV/s), [e] Anodic current, [f] in KBr pellet, [g] wavenumber in cm^{-1} .

Table 4 Quenching constant (K_q), binding constant (K_{bin}), number of binding sites (n) and the values of the apparent association constant (K_a) for the interactions of complexes **1** and **2** with BSA/HSA.

Complex	K_{sv} (M^{-1})	K_q ($M^{-1}S^{-1}$)	K_{bin} (M^{-1})	n	K_a (M^{-1})
BSA 1	9.51(± 0.09) $\times 10^4$	1.90(± 0.09) $\times 10^{13}$	8.51(± 0.01) $\times 10^4$	0.79	9.50(± 0.07) $\times 10^2$
2	7.99(± 0.01) $\times 10^4$	1.59(± 0.01) $\times 10^{13}$	7.58(± 0.02) $\times 10^4$	0.73	6.63(± 0.07) $\times 10^2$
HSA 1	7.45(± 0.07) $\times 10^4$	1.49(± 0.07) $\times 10^{13}$	7.17(± 0.02) $\times 10^4$	0.83	6.19(± 0.09) $\times 10^3$
2	5.12(± 0.06) $\times 10^4$	1.02(± 0.06) $\times 10^{13}$	6.30(± 0.03) $\times 10^4$	0.76	3.47(± 0.11) $\times 10^3$

Table 5 Electronic spectral parameters of complexes **1** and **2** bound to CT-DNA.

	λ_{\max} (nm)	change in emission	$\Delta\epsilon$ (%)	K_{sv} (M^{-1})	K_{ib} (M^{-1})	K_{app} (M^{-1})
1	602	hypochromism	63.13	1.483(± 0.11) $\times 10^5$	1.25(± 0.22) $\times 10^4$	8.86 $\times 10^5$
2	602	hypochromism	59.09	9.78(± 0.08) $\times 10^4$	8.77(± 0.10) $\times 10^3$	7.14 $\times 10^5$

Table 6 Kinetic parameters of the interaction of Cu(II) cubane compounds with CT-DNA.

Compound	K_{ib}	K_{sv}	Ref.
$[Cu_4(L)_2(HL)_2(H_2O)_2] \cdot 2(ClO_4) \cdot DMF$ (1)	1.25 $\times 10^4$	1.483 $\times 10^5$	This work
$[Cu_4(L)_2(HL)_2(H_2O)_2] \cdot (tp)$ (2)	8.77 $\times 10^3$	9.78 $\times 10^4$	This work
$Cu_4(L^1)_4$	4.50 $\times 10^3$	-	[3g]
$[Cu_4(\mu-L^2)_2(\mu_{1,1,3,3}-O_2CH)](OH) \cdot 6H_2O$	3.37 $\times 10^4$	4.73 $\times 10^4$	[3h]
$[Cu_4((HL^3)_2(H_2L^3)_2(H_2O)(C_2H_5OH))] \cdot 2(ClO_4) \cdot 2(C_2H_5OH)$	1.35 $\times 10^4$	1.69	[3i]
$[Cu_4(H_2L^4)_4 \cdot 2H_2O] \cdot 5H_2O$	1.48 $\times 10^4$	-	[3j]
$[Cu_4(H_2L^4)_4 \cdot 4H_2O]$	2.54 $\times 10^4$	-	[3j]

H_2L^1 = Schiff base of 1-amino-2-propanol and salicylaldehyde; H_3L^2 = 1,3-bis [3-aza-3-(1-methyl-3-oxobut-1-enyl)prop-3-en-1-yl]-2-(2-hydroxyphenyl)-1,3-imidazolidine; H_3L^3 = 2-ethyl-2-((2-hydroxy-3-methoxybenzylideneamino)propane-1,3-diol); H_4L^4 = 2-[(2-hydroxy-3-methoxy-benzylidene)-amino]-2-hydroxymethyl-propane-1,3-diol.

Captions of the Figures

Fig. 1. Molecular structure of **1** (lattice DMF, H_2O molecules and hydrogen atoms are omitted). Only one out of the two orientations of the disordered perchlorate anion and one out of two disordered $-CH_2-CH_3$ side chains of the three Schiff base ligands are shown for clarity.

Fig. 2. Molecular structure of **2**. The hydrogen atoms are omitted for clarity.

Fig. 3. Simplified representation of the tetranuclear copper(II) core in **1**.

Fig. 4. 1D supramolecular structure of **2** formed by hydrogen bonding interactions with the lattice terephthalate anion.

Fig. 5. Plot of $1/[complex]$ vs $1/(A_{obs}-A_0)$ for the interactions of complexes **1** and **2** with serum albumins.

Fig. 6. Fluorescence spectra of BSA ($\lambda_{ex} = 280$ nm; $\lambda_{em} = 340$ nm) and HSA ($\lambda_{ex} = 280$ nm; $\lambda_{em} = 330$ nm) in the presence of increasing amounts of complex **1** [(A) for BSA, (B) for HSA] and complex **2** [(C) for BSA, (D) for HSA]. Arrows show the emission intensity changes upon increasing the complex concentration. Inset: Stern-Volmer plot.

Fig. 7. Scatchard plots for complexes **1** and **2** with BSA / HSA. (Here $[complex]$ is the total concentration of the added complex).

Fig. 8. Absorption spectra of complexes [(A) for **1** and (B) for **2**] in the absence (black line) and in presence (other lines) of increasing amounts of CT-DNA, at room temperature. Inset:

show the plots of $[DNA]/(\epsilon_a - \epsilon_f)$ vs. $[DNA]$. The arrows show the absorbance change with increasing CT-DNA concentration.

Fig. 9. Effect of addition of complexes **1** (A) and **2** (B) on the emission intensity of EB bonded CT-DNA. Inset: Stern-Volmer plots of the fluorescence titrations.

Fig. 10. Cyclic voltammograms of **1** (black) and **2** (red).

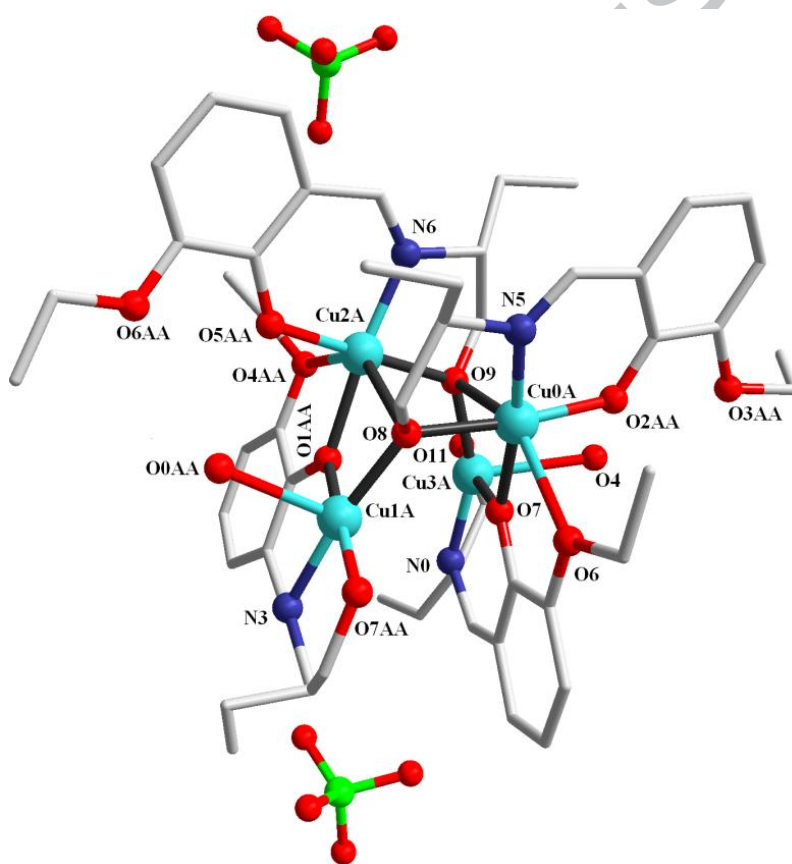


Fig. 1

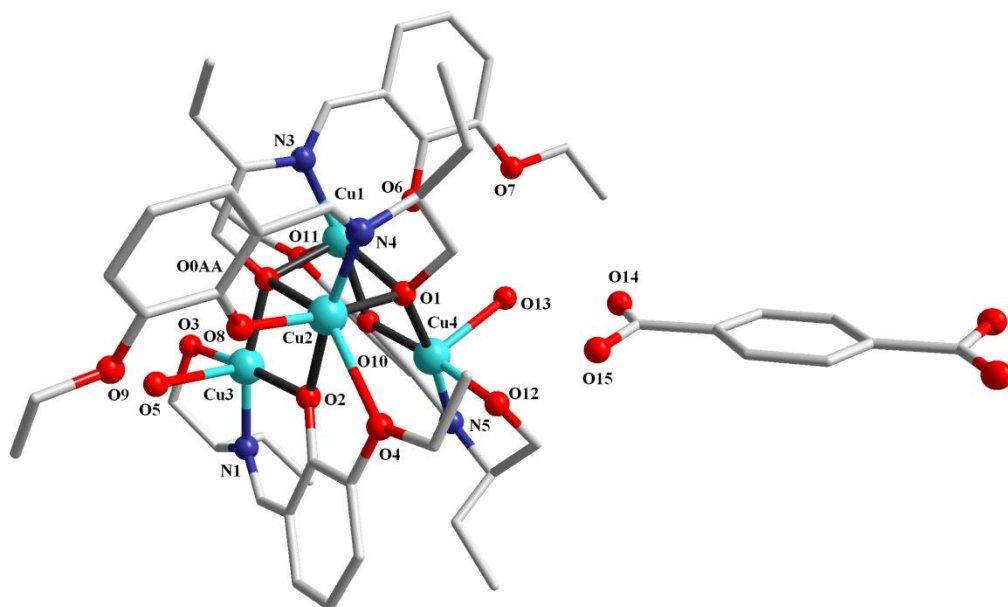


Fig. 2

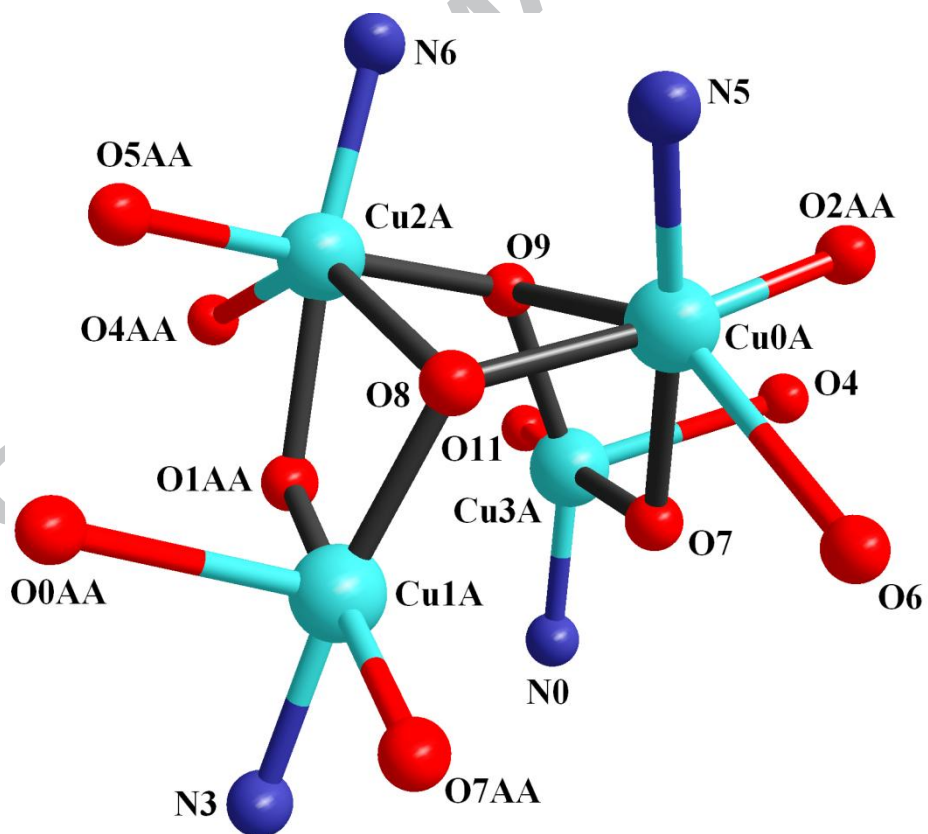


Fig. 3

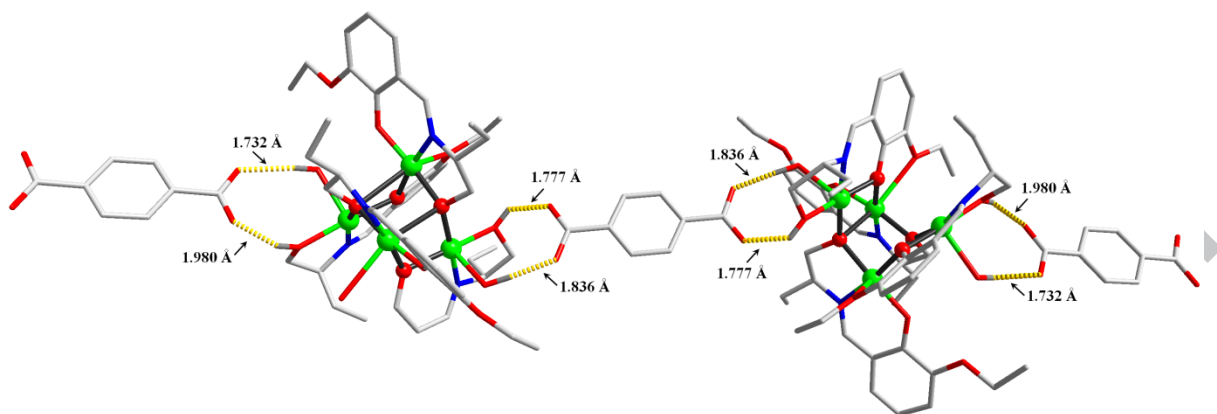


Fig. 4

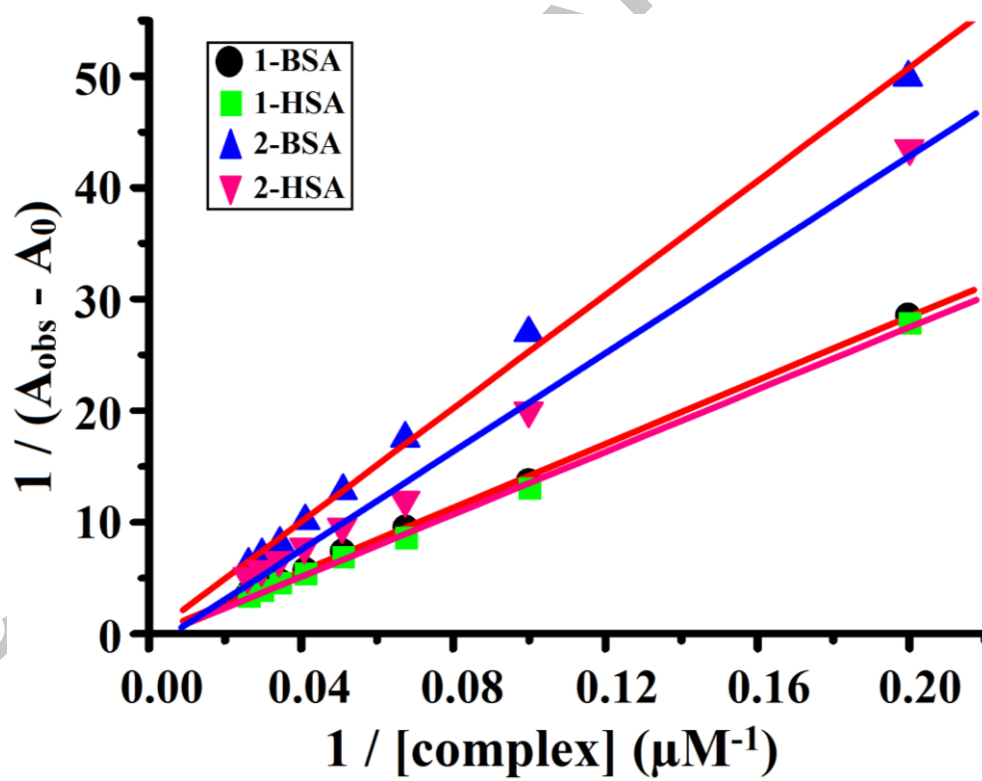


Fig. 5

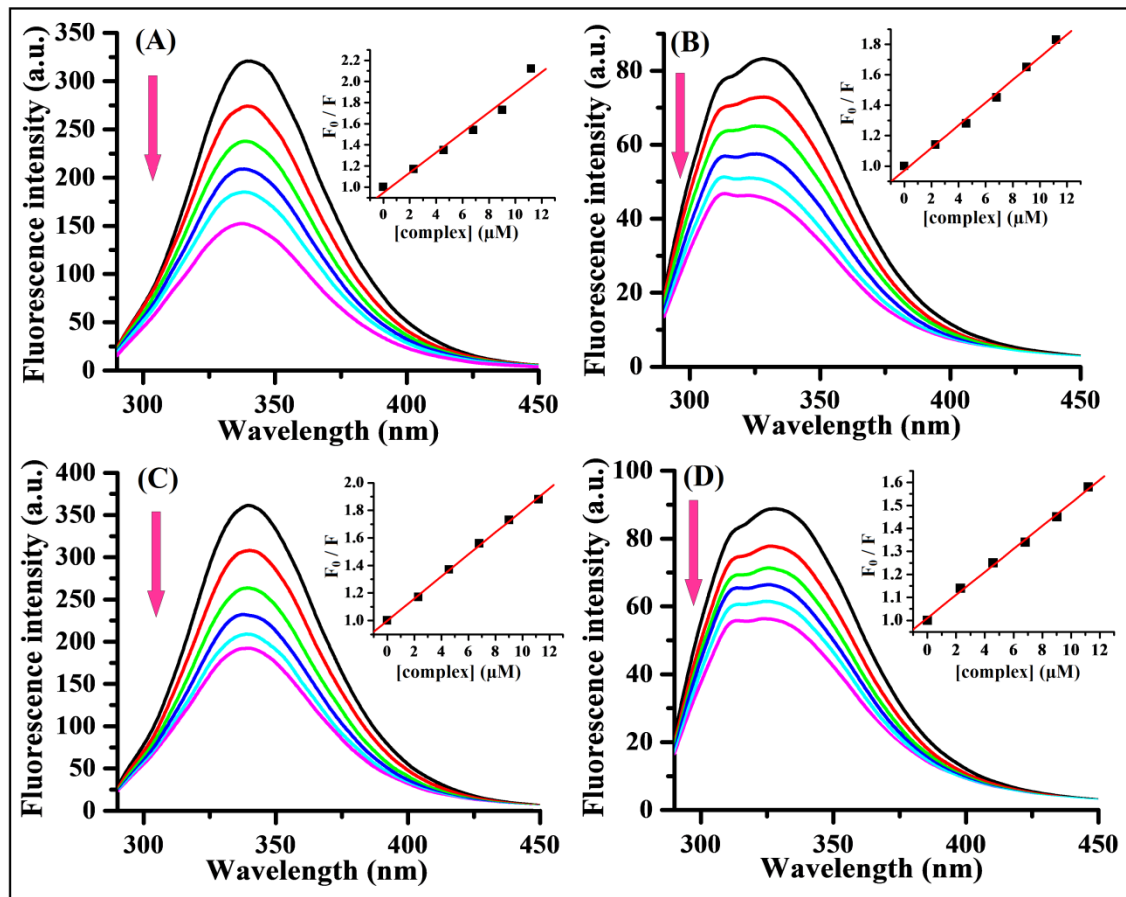


Fig. 6

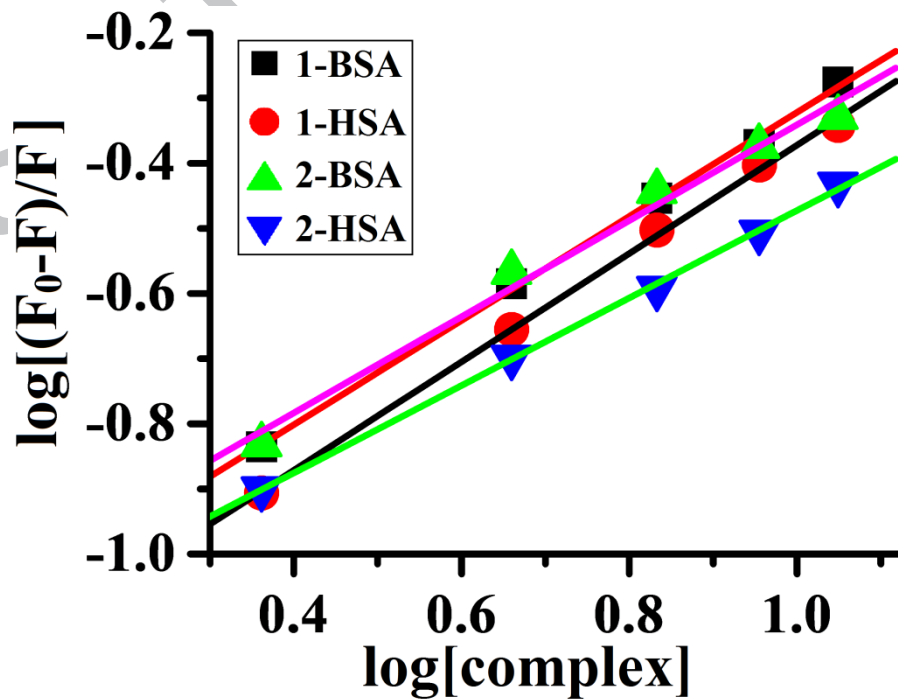


Fig. 7

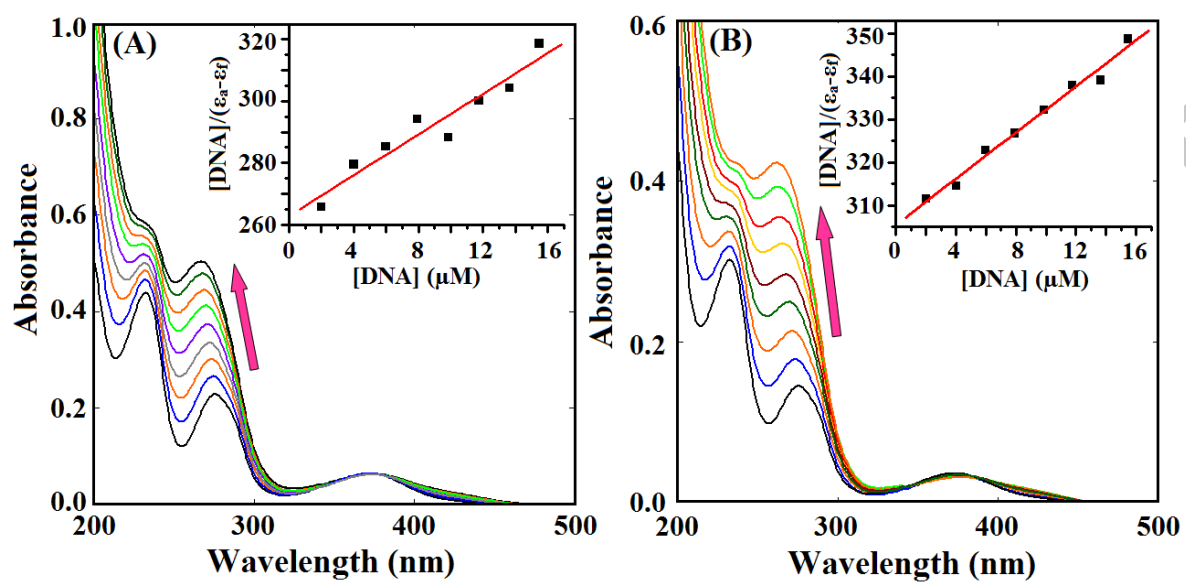


Fig. 8

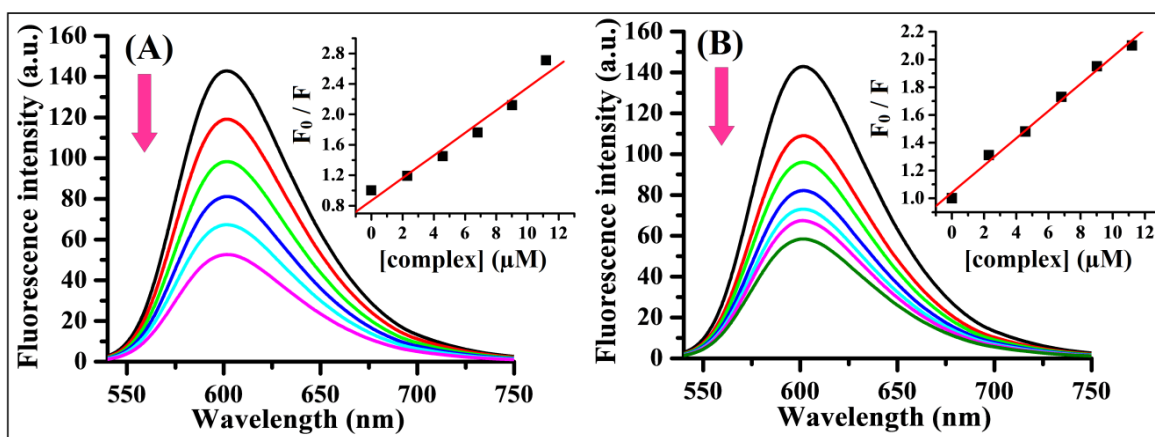


Fig. 9

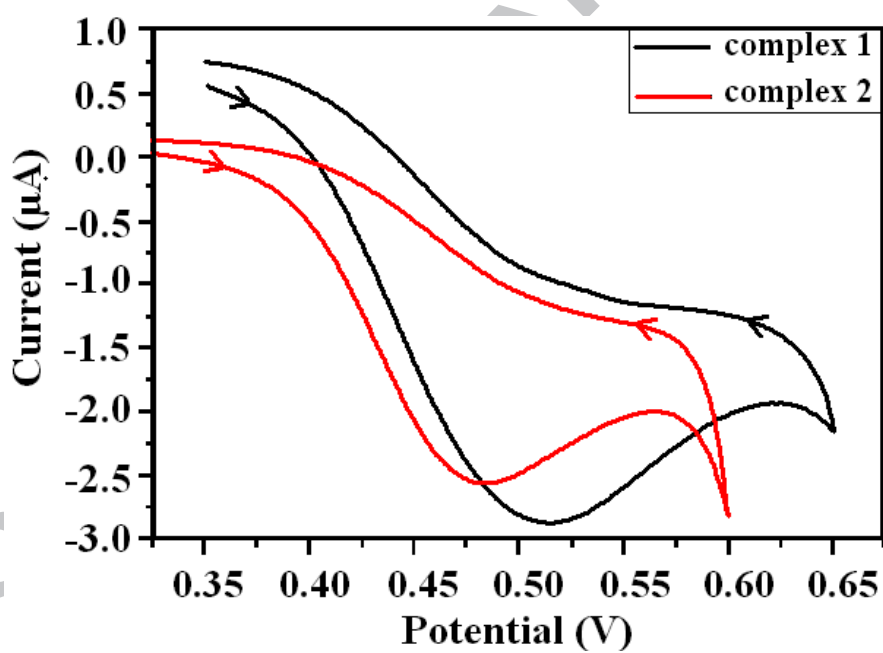
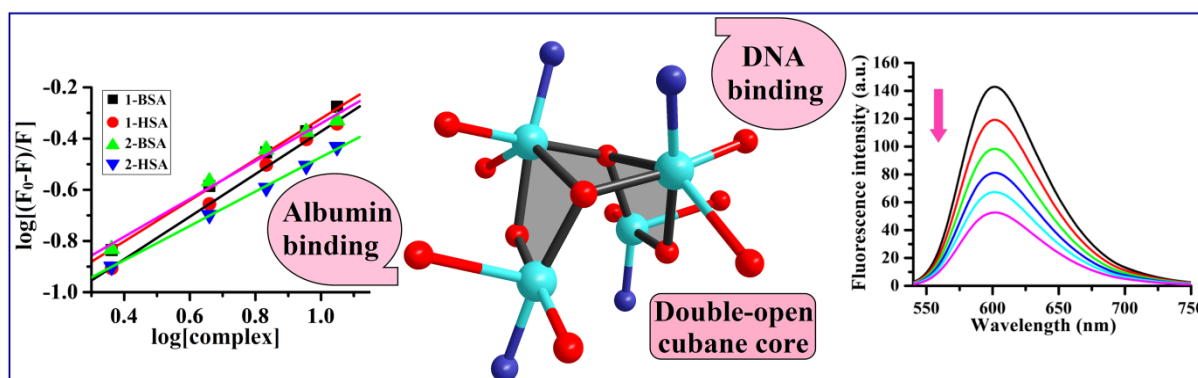


Fig. 10



Tetranuclear Cu(II) complexes with double-open-cubane like core frameworks were synthesized and characterized by crystal structure analysis. Interactions of the complexes with serum albumins and CT-DNA were studied using electronic absorption and fluorescence spectroscopic techniques.